Automatic differentiation of human induced pluripotent stem cells toward synchronous neural networks on an arrayed monolayer of nanofiber membrane

Boxin Huang, Yong He, Elrade Rofaani, Feng Liang, Xiaochen Huang, Jian Shi, Li Wang, Ayako Yamada, Juan Peng, Yong Chen

Automatic differentiation of human induced pluripotent stem cells toward synchronous neural networks on an arrayed monolayer of nanofiber membrane

Boxin Huang [a], Yong He [a], Elrade Rofaani [a], Feng Liang [a], Xiaochen Huang [a], Jian Shi [b], Li Wang [b], Ayako Yamada [a], Juan Peng [a]*, Yong Chen [a]*

[a] PASTEUR, Département de chimie, École normale supérieure, PSL University, Sorbonne Université, CNRS, 75005 Paris, France

[b] MesoBioTech, 231 Rue Saint-Honoré, 75001, Paris, France

E-mail: yong.chen@ens.psl.eu, juan.wang@ens.psl.eu

Keywords: hiPSCs, cortical neural networks, guided self-organization, automated differentiation

Cortical neural networks can be differentiated from human induced pluripotent stem cells (hiPSCs) and studied toward a comprehensive understanding of brain functions. Herein, we present a method to guide the self-organization of differentiating neural cells with an arrayed monolayer of nanofiber membrane and an automatic culture system. The nanofiber membrane was obtained by electrospinning and chemical crosslinking of gelatin nanofibers on a patterned honeycomb frame. Neural precursor cells (NPCs) derived from hiPSCs were seeded on the membrane to form self-organized and inter-connected neural clusters in each of the membrane areas. Compared to other types of culture substrates, the arrayed nanofiber membrane is advantageous in terms of the biocompatibility of stiffness and permeability to neurons. Thus, the resulted clusters on nanofiber-membrane showed dense neural connectivity, low glia-neuron ratio, regular distribution, and enhanced neural activities. Our results also demonstrated that the automatic culture system was enabling not only for manpower saving but also for avoiding undesired disturbing on the neural networks under development. Synchronous neural activity and increased synaptic number, area, and population fully revealed the benefits of the automated differentiation method. Combining the nanofiber membrane and automated method is a practical approach and enables further cortical neural function studies.

1. Introduction

Human-induced pluripotent stem cells (hiPSCs) can be self-renewed and differentiated into cortical neural cells, offering unprecedented opportunities for in vitro modeling of brain functions [1-6]. Of interest is the generation of cortical neural networks with synchronized activities which are essential for neural information processing and human cognition [7,8]. While synchronization is generally observed in the electrical activity between various brain regions, it can also be recorded with a group of interconnected neural cells [9-16]. In this regard, the emergence of synchronized activities should be considered as a criterion of a mature neural network and it is important to develop more systematic investigations along this line. During the last years, various protocols have been proposed including organoid-type differentiation [2,3], directed differentiation [4,5], and lineage-specific differentiation [6,17,18] but few of them allowed to generate cortical neural networks with synchronized activities.

Typically, hiPSCs are firstly derived to neural progenitor cells with a commitment then subjected to a long-term differentiation by either suspension or adherent cell culture. Brain organoids are generally obtained by suspension culture and used for studies of early human brain development and brain diseases [3,4,19-21]. The drawback of this approach is that the produced organoids are generally small, immature, and not well-defined due to lack of vasculature and lack of precise control of the cell organization [22,23]. Cortical neural networks can be achieved by directed or lineage-specific hiPSC differentiation on a substrate. The advantage of directed differentiation relies on the generation of the network with multicellular types including neurons and astrocytes [4,5], while lineage-specific differentiation requires an additional step of cell mixing and coculture of derives neurons and astrocytes to form a functional neural network. Overall, the directed differentiation is relatively simple which can also benefit advantages of material engineering, neural signal recording, microfluidic integration, and high throughput screening.

To improve the performance of differentiated neural networks, a variety of culture conditions have been studied by considering the effect of stiffness, surface morphology, and coatings of the substrate [24-26]. For example, hydrogels [27,28] and micro-pillars [29-31] were used as low stiffness substrates for neural differentiation of hiPSCs. Random and aligned nanofibers [32-34], patterned substrates [35-37], microfluidic channels [38-42], and three-dimensional (3D) structures [43-47] were

explored for the control of neurite outgrowth and the formation of neural networks. These approaches are intuitive but they were mostly limited to the proof-of-concept and the formation of randomly organized neural networks. We have recently proposed a new type of culture device consisting of a monolayer of crosslinked gelatin nanofibers on a patterned honeycomb frame (culture patch) [48,49]. Such a culture device is advantageous over conventional culture devices since the culture support is now made of a natural biopolymer and it is inherently low stiffness and high permeability. Primary hippocamp cells could be cultured, showing in-vivo like astrocyte morphology and enhanced neural activities compared to that on a glass slide [50]. By depositing the monolayer of nanofibers on both sides of the frame, a new type of bilayer scaffolds could be obtained for three-dimensional (3D) cell culture [51]. Most recently, we demonstrated the formation of regular 3D neural clusters in a bilayer scaffold for the observation of neuronal synchronization and a brain-blood barrier like organization [52]. It is however not clear whether the neuronal synchronization can be can be achieved with a two-dimensionally patterned substrate. This article describes such a study by comparing three types of substrates and two types of differentiation methods. We first compare the performance of hiPSC differentiation on glass, nanofiber-covered glass, and nanofiber membrane to demonstrate the advantages of the nanofiber membrane. Then, we compare the performance of manual and automated differentiation to demonstrate the necessity of avoiding the culture system instability during the long period of hiPSC differentiation processing. Our method is simple and shows potential of generating regular and synchronized cortical neural clusters for future studies.

2. Materials and method

Reagents were purchased from Sigma-Aldrich unless otherwise specified.

2.1 Fabrication of the substrates

Arrayed nanofiber membranes were fabricated by using the protocol previously reported [38,39]. Briefly, a master pattern of microframe was prepared by using a two-level photolithography with SU8 negative resist (Micro Resist Technology) spun coated on a silicon wafer, giving rise to a honeycomb structure of 200 μm thick, 200 μm bandwidth and 500 μm compartment size (vertex-vertex distance) with a support ring of 7 mm inner and 13 mm outer diameter. After being exposed to the vapor of

chlorotrimethylsilane (TMCS), a solution of PDMS prepolymer and crosslinker (RTV 615, Neyco) mixture at a ratio of 10:1 (w/w) was poured on the SU8 mold, degassed, and polymerized at 80 °C for 2 h. The resulted PDMS block was then placed on a glass slide with the structured-side down and kept under vacuum for 10 min immediately before injecting a low viscous and UV sensitive resist, OrmoStamp (Micro Resist Technology). Once fulfilled, UV exposure was applied at 21.6 $mW \cdot cm^{-2}$ light intensity for 2 min. After being peered off, the OrmoStamp honeycomb structure together with a ring is coated with 10 nm-thick gold and then used as a collector for electrospinning deposition of gelatin nanofibers.

Gelatin from porcine skin was dissolved at 15 wt% in a solvent mixture containing distilled water, ethyl acetate, and acetic acid at a volume ratio of 10:14:21 and used in 2 days. The gelatin solution was ejected at a flow velocity of 0.2 $mL \cdot h^{-1}$ by a syringe pump (Harvard Apparatus) from an anode syringe needle to the glass substrate placed on a cathode collector at a distance of 10 cm from the needle under a bias voltage of 11 kV. Gelatin nanofibers were electrospun for 5 min. After removing the residual solvent in a desiccator, nanofibers were crosslinked in 0.2 M N-(3-Dimethylaminopropyl)-N'-ethylcarbodiimide hydrochloride and 0.2 M N-hydroxysuccinimide in ethanol at room temperature for 4 h. Finally, samples were rinsed with ethanol three times, dried under the vacuum, and stored in a cool and dry place. The same electrospinning and chemical crosslinking parameters were used for the fabrication of nanofiber-covered glass substrates. Glass substrates were prepared using standard glass clean procedure, i.e., ultrasonic clean with acetone, hot trichloromethyl clean, DI water clean, and drying in an oven.

2.2 Permeability and stiffness assays

The permeability of membrane, κ, is reversely proportional to the flow resistance of the membrane, R_m. According to Darcy's law [53], $\kappa = \mu L / R_m A$, where μ is the dynamic viscosity of the fluid, L *is* the thickness, and A is the area of the membrane. By measuring the flowrate as a function of pressure, R_m can be determined [54]. This was done by inserting a membrane inside a microfluidic device (MesoBioTech, France) and measuring the flowrate of DI water crossing the membrane as a function of pressure, from which the flow resistance of the system with membrane R_s can be calculated. Similarly, the flow resistance of the system with a bare frame R_f can be

obtained. Since $R_m = R_s - R_f$, κ, can be deduced for given μ, L, and A of the membrane.

The effective Young's modulus of the nanofiber membrane was determined by measuring the deflection of the membrane area in a similar way of [55] by slightly modified. Briefly, a solution of concentration agarose was dropped on the nanofiber membrane and dried for hydrophobic surface coating. The membrane was then inserted into a microfluidic device. DI water was injected into the chambers separated by the membrane with a controlled pressure. The pressure induced membrane deflection was carefully observed with an optical microscopy (Zeiss Axio-Observer Z1, Germany) by measuring the focal plans of the maximum (in the center of each membrane area) and minimum (frame area) deflection, the difference in Z was recorded as a function of applied pressure and then fitted by using an analytic formula as described in [55].

2.3 Cell adhesion assay

Substrates of arrayed nanofiber-membrane, nanofiber-covered glass, and glass slide of the same diameters were attached on a 60 mm diameter Petri dish at a distance of 1 cm from the center. After sterilization by 70 % ethanol and UV exposure, 2 mL diluted Geltrex solution (1:100, Thermofisher Scientific) were injected for coating at 37 ºC for 1 h. Next, 3.5×10^4 NIH-3T3 cells (93061524) were seeded onto each substrate and incubated in MEM medium supplemented with 10 % FBS and 1% Penstrep (Thermofisher Scientific) for 4 h. In order to count cell number more easily, cell nuclei were labeled by Hoechst (5 μg·mL^{-1}, Thermofisher Scientific) in 37 ºC, 5 % CO_2 incubator for 30 min. Then, the Petri dish was partially filled with culture medium and centrifuged at 2000 rpm for 30 s by a spin coater. The remained cells were analyzed with an inverted microscopy (Axio Observer Z1, Zeiss) and the cell number was counted semi-automatically by Fuji/image J software (2.1.0, USA) [56].

2.4 Deflection and stiffness of nanofiber membrane

Similar to the previous work of [55], an arrayed nanofiber membrane was integrated into a microfluidic device and DI water was injected into the basal part of the chamber separated by the membrane. Before integration, the surface of the nanofibers of the membrane were coated with 2 wt% agarose to prevent leakage. The displacements of the center and the edge part of the membrane were then measured as

a function of pressure applied to basal apart of the chamber, by using the inverted optical microscopy (Axio Observer Z1, Zeiss). The deflection with a given pressure was obtained by calculating the difference of the displacement between the center and the edge parts. By data fitting based on a flat theory [55], the effective Young's modulus of the nanofiber membrane could be deduced.

2.5 Generation of neural precursor cells

The stepwise differentiation of hiPSCs to cortical neural networks could be divided into two stages. Firstly, NPCs which were capable to be differentiated into neurons and glial cells were derived from hiPSCs. Then, NPCs were differentiated into multicellular systems on three types of substrates. Typically, the hiPSC-derived NPCs can be self-renewed and cryopreserved for later uses, while the differentiation of NPCs needs a longer period of culture. The detailed process and parameters of the NPCs were shown in Fig. 2A. hiPSCs (A18945, Episomal line, Life Technologies, France) were cultured with Essential 8 Flex Medium (E8F, Thermo Fisher Scientific) on a tissue culture dish, which was treated with 5 $\mu g \cdot mL^{-1}$ vitronectin (VN, Thermo Fisher Scientific) in PBS for 1 h in 37 °C, 5 % CO_2 incubator prior to use. The hiPSCs were subsequently differentiated into NPCs by following the protocol described with a slight modification [5]. Firstly, dissociated hiPSCs were seeded on a non-attachment round-bottom 96 well plate (Corning) at a cell density of 5000-10,000 per well, and allowed to form embryoid bodies (EBs) in E8F for 2 days. The culture medium was then switched to neural induction medium (NIM) composed of DMEM/F12 medium, 1 % N2 supplement (Thermo Fisher Scientific, France), 2 $\mu g \cdot mL^{-1}$ heparin (Stemcell, France), and 1 % Pen-strep, in which cells were cultured for 4 days. On day 7, 6-10 EBs were transferred on each well of 12-well plate, which was incubated with 20 $\mu g \cdot mL^{-1}$ laminin in PBS for 1 h at 37 °C beforehand, and cultured in NIM until day 14 to generate pre-NPCs. Pre-NPCs were then cultured in neuronal precursor medium (NPM) composed of DMEM/F12 medium, 1 % N2 supplement, 2 % B27 minus vitamin A supplement (Thermo Fisher Scientific, France), 1 $\mu g \cdot mL^{-1}$ laminin, 20 $ng \cdot mL^{-1}$ bFGF, and 1 % Pen-Strep from day 15 onward. The medium was renewed every 2 days and cells were sub-cultured on a dish treated with 1% Geltrex (LDEV-free, reduced growth factor, Thermo Fisher Scientific) in DMEM/F12 medium for 1 h

at 37 °C when confluent. Afterward, the cells were collected for passages as derived below.

Cells were brought into suspension using TrypLE (Thermo Fisher Scientific) or Accutase (Thermo Fisher Scientific), incubated for 5 min at 37 °C with 5% CO_2, and then resuspended in a volume of fresh DMEM/F12 Medium at least equivalent to the volume of TrypLE or Accutase. After centrifuging at 1000 rpm for 5 min, cells were resuspended in NPM and seeded with the desired number onto the Geltrex coated culture dish. After 5 passages, cells were considered as NPCs. To cryopreserve NPCs, a commercial procedure for cell lines cryopreservation was applied. Here, cells after day 15 of confluence were placed in a cryoprotective ampoule at a concentration of 1-4×10^6 per ml and a freezing medium composed of 10 % DMSO in NPM was used. Similarly, after being thawed, the NPCs need 2 passages before differentiation.

2.6 Differentiation of neural networks on substrates

Prior to cell seeding, substrates were treated by air plasma (Harrick Plasma) for 1 min and sterilized by UV irradiation in 70 % ethanol for 30 min. After being rinsed with PBS three times and dried at room temperature, the substrates all were incubated with 50 µL 100 $\mu g \cdot mL^{-1}$ poly-L-ornithine at 4 °C overnight or at room temperature for 2 h and rinsed 3 times with PBS. Next, a droplet of 1% Geltrex (50 µL) in DMEM/F12 medium was deposited on each substrate and then incubated for 1 h in a humidified incubator at 37 °C. Subsequently, NPCs were detached using Accutase, seeded on the coated sides of three types of substrates at a density of 3×10^5 per substrate, incubated for 2 h at 37 °C and 5% CO_2 incubator for cell adhesion, and kept culturing in 1 mL NPM. Finally, NPCs were cultured in neural differentiation medium (NDM) composed of Neurobasal medium (Thermo Fisher Scientific) supplemented with 1 % N2 supplement, 2 % B27 minus vitamin A supplement, 20 $ng \cdot mL^{-1}$ brain-derived neurotrophic factor (Stemcell), 20 $ng \cdot mL^{-1}$ glial cell-derived neurotrophic factor (Stemcell), 1 % MEM non-essential amino acids solution (Thermo Fisher Scientific), 1 µM dibutyryl cyclic adenosine monophosphate, 2 $\mu g \cdot mL^{-1}$ laminin and 1 % Pen-strep. NDM was renewed every two days for 4 weeks and then 50 % renewed every two days for the rest of the time.

2.7 Development of automated differentiation system

The system is composed of a storage unit, a pump unit, and a cell culture unit, all controlled with a PC or an Arduino board (Fig. 4B-C). The storage unit was placed in a 4°C fridge to maintain the bioactivity of soluble factors. The associated electromagnetic valve was switched on only when the medium was pumped out. The culture unit consists of six independent pipelines for injection and extraction of culture

medium. In this work, 60 mm diameter culture dishes and adapted cover-plates were used (C1-C6). The injection and extraction of the medium were controlled with two rotational switches (R1, R2). The fluidic connections between rotational switches, culture dishes, peristaltic pumps, medium supply and waste were done with silicone tubes and Luer connectors (MesoBioTech, France), as schematically shown in Fig. 4B. To complete the medium replacement in a dish, peristatic pump P2 firstly moves out the used medium from the dish to the waste and then peristatic pump P1 moves the fresh medium from the storage bottle to the dish. The two rotational switches are synchronized for a dish and the medium change can thus be performed step by step for all six dishes. If the neural networks in one dish become matured, the dish can be replaced by a new one so that the system can work continuously (Fig. 4C). More detailed description on the dish cover plate and other components can be found in [57].

Before use, the automated system should be sterilized. Firstly, the bottles for medium storage and collection were sterilized with an autoclave and the surface of the automated system was wiped by 70 % ethanol and sterilized in the bio-batch under the UV light for 30 min. All the tubes, Luer connectors, and lids were fully dipping in 70 % ethanol. Secondly, the automated system was assembled and washed again by flowing 70 % ethanol, sterilized PBS with 1 % PS and DMEM/F12 medium plus 1 % PS into all pipelines and containers of the system. This washing step could be done automatically with the control unit with a dedicated program sequence. This washing cycle of 70 % ethanol was repeated twice and the ethanol solution was collected in a sterilized bottle. The commercial falcon tubes were used here as temporary containers. Finally, the pipelines and containers for washing were replaced by a new set of sterilized ones.

2.8 Automated differentiation of NPCs to cortical neural networks

The protocol of manual and automated differentiation is shown in Fig. 4A. The preparation of nanofiber-membrane and the seeding process of NPCs are the same as described in 2.5 and 2.6. 2 h after cell seeding, NPCs on-substates were transferred into 12 well plate or a patch fixing mold in a 60 mm petri dish for further differentiation by the manual and automatic method, respectively. Six culture devices with NPCs were differentiated towards cortical neural network together in one 60 mm petri dish. Once these processes were finished, the automatic program started to run. 1 mL and 6 mL NDM were added into each 12 well plate and the petri dish, respectively. Sufficient NDM was prepared in previous and filled into the medium storage bottle for automated differentiation (Fig. 4B). Later, NDM was fully renewed every two days for 30 days and half of the volume was renewed onwards. For automated system, the medium

replacing step is accurate to the hour, while is accurate to the day by the manual medium change method.

2.9 Scanning electron microscopy (SEM) observation

Firstly, a 5 nm-thick gold layer was sputtered on the nanofiber layers which covered onto glass and honeycomb frame. Next, samples were observed by SEM (Hitachi TM3030) operated at 10 kV.

2.10 Immunofluorescence staining

Cells were fixed by incubating them in 4 % (w/v) paraformaldehyde for 15 min, followed by permeabilization in 0.5% (w/v) Triton X-100 in PBS for 10 min and incubation in a blocking solution (3% bovine serum albumin, 0.1% Tween 20, and 0.1% sodium azide (w/v) in PBS) for 30 min at room temperature. The samples were further incubated with primary antibodies at 4 °C overnight, prior to incubation with secondary antibodies in the blocking solution for 2 h and subsequent cell nuclei staining in PBS containing 1 $\mu g \cdot mL^{-1}$ DAPI for 15 min at room temperature. The following primary antibodies were used for immunostaining: anti-Nestin (N5413, Sigma-Aldrich, 1:100), anti-βIII tubulin III (T8578, Sigma-Aldrich, 1:500), anti-GFAP (MA5-12023, Thermo Fisher Scientific, 1:100), anti-GFAP (180063, Invitrogen, 1: 100), anti-Neurofilament 200 (N4142, Sigma-Aldrich, 1:80) anti-MAP2 (13-1500, Thermo Fisher Scientific, 1:250), anti-Tau (T9450, Sigma-Aldrich, 1:100), anti-Synapsin I (ab64581, abcam, 1:200). Alexa fluor 488 anti-mouse (A-21200, 1:500), Alexa fluor 555 anti-mouse (A21147, 1:500), Alexa fluor 633 anti-mouse (A-21050, 1:500), Alexa fluor 488 anti-rabbit (A32790, 1:500), Alexa fluor 555 anti-rabbit (A31572, 1:500) and Alexa fluor 633 anti-rabbit (A21070, 1:500) antibodies (all from Thermo Fisher Scientific) were used as secondary antibodies. Fluorescently labeled cells were imaged by confocal microscopy (LSM 900, Zeiss).

2.11 Image acquisition and analysis

For fluorescence analysis of neural clusters, cell nuclei staining images obtained by confocal microscopy were processed by background subtraction and standardized thresholding (default) with Fiji/ImageJ software (USA) [56]. Then, the intensity of ROIs was calculated with the plugin module ‘Mean Grey Value’. The ROIs and the size of neural clusters (Fig. 2G, 2H), were obtained by ImageJ Particles Analysis. In Fig. 3C, the fluorescence on the frame area were excluded and same areas of two

independent experiments were selected for further calculation. Glia-neuron ratio of each neural networks was calculated based on the number of $GFAP^+/NF200^-$ and $NF200^+/GFAP^-$ labeled cells in each fluorescent image. In addition, the area size and number of synapsin I spots per 0.045 mm^2 were analyzed by the Particle Analysis function of Fuji/image J software (2.1.0, USA) [56] and threshold selection was performed using a Renyi entropy-based method (Fig. 4F).

2.12 Calcium imaging analysis

Cells were rinsed with a recording buffer (145 mM NaCl, 3 mM KCl, 1.5 mM $CaCl_2$, 1 mM $MgCl_2$, 10 mM glucose, and 10 mM HEPES, pH 7.4) and incubated in the recording buffer with 2 μM Fluo-4 AM and 20 % pluronic acid (both from Thermo Fisher Scientific) at 37 °C in a 5% CO_2 incubator for 25 min. After incubation, the samples were rinsed with the recording buffer twice and transferred to the stage of an inverted fluorescence microscope (Axio Observer Z1, Zeiss) equipped with an Electron Multiplier CCD Camera C11440 (Hamamatsu Photonics). Further, each frame was acquired every 500 ms for 10 min and analyzed using a MATLAB program named FluoroSNNAP (Fluorescence Single Neuron and Network Analysis Package) by MATLAB software (USA) [58] or semi-automatic manner. The package allowed semi-automated identification of ROIs and calculation. The fractional optical signal was calculated as follow: $\Delta F/F = (I_f(t) - I_f(t_0)) / I_f(t_0)$, where $I_f(t_0)$ is the average fluorescence intensity of the lower 50% of previous 10-s values and I_f (t) is the time course of the fluorescence intensity in an ROI. Raster plot displaying the calcium activities was used to investigate the synchrony in the neural networks. More than three samples of each substrate were recorded and verified.

To investigate the activity of neural networks on the suspended nanofibers with and without glucose, calcium transients of cells were first recorded under the no-glucose condition by removing the glucose from the recording buffer. Later, a fresh recording buffer containing 10 mM glucose replaced the previous no-glucose buffer, and the same areas of signal transmissions were continued to record.

2.13 Statistics

Data are shown as the mean ± SEM from at least three samples. For the analysis, n refers to the number of samples. The conclusion of significant differences among three types of substrates are based on the analysis of one-way ANOVAs. The quantified analysis between two groups (nanofiber membrane vs nanofiber glass; manual vs automatic method) was analyzed with Student's-t-test. GraphPad Prism software (GraphPad 9.0, USA) was used for statistical analyses. The number of

replicates and statistical tests used for each experiment are mentioned in the respective Fig. legends. Significance was set to $^{*}P< 0.05$, ** $P< 0.01$ and *** $P< 0.001$.

3. Results

3.1 Substrate of arrayed monolayer nanofiber membrane

By using electrospinning and chemical crosslinking techniques, a monolayer of crosslinked gelatin nanofibers was deposited on a patterned honeycomb microframe (Fig. 1A-C). Similarly, a nanofiber covered glass was obtained, showing comparable morphologies with an averaged nanofiber diameter of 520 ± 270 nm (n=6) and a porosity of 15.8± 2.2 %. Statistically, 90.6%, 6.8% and 2.6% of pores have small (0-10 μm^2), middle (10-20 μm^2) and large pore areas (20-80 μm^2), respectively (Fig. 1D). The porosity of the nanofiber membrane was reduced by ~3.5 % after immersion in PBS for 10 min and remained unchanged. Fig. 1E shows the flowrate as a function of pressure of a bare frame and a nanofiber membrane from which a flow resistance of 1.50 ± 0.05 mbar·min·mL^{-1} and 0.62 ± 0.03 mbar·min·mL^{-1} were deduced. With the geometry parameters of the frame, an effective membrane thickness of 367 nm, and a viscosity of DI water of 8.9×10^{-4} N·s·m^{-2}, a permeability 537 nm² could be deduced. The wetting property of the nanofiber membrane was also determined by measuring the contact angle of DI water, PBS, and culture medium, which are 65°, 51° and 70° respectively [59,60]. Finally, the cell adhesion on different types of substrates is compared by measuring the remained cell numbers after spinning treatment(Fig. S1A), indicating a much higher adhesion strength of the cells on nanofiber type substrates than that on a glass substrate (Fig. 1F).

The stiffness of the nanofiber membrane was determined in a similar way as described in [54]. As can be seen in Fig. 1G, the deduced effective Young's modulus of the nanofiber membrane E_s = 2.0 MPa is smaller than of a 50 µm and 100 µm thick PDMS membranes [55]. Moreover, the effective in-plan and out-of-plane Young's modulus can be estimated by considering a hexagonal mesh of lattice parameter of l and thickness of t with a material Young's modulus of E_s. which is given by $\frac{4\sqrt{3}}{3}E_s(t/l)^3$ and $\frac{2\sqrt{3}}{3}E_s(t/l)$, respectively [61]. Assuming a ratio of t/l = 0.05, we obtained an effective in-plane Young's modulus ~ 0.57 kPa, which is close to the Young's modulus of neural tissues [62]. Obviously, the Young's modulus of nanofiber

covered glass is close to that of the glass and in the order of GPa. Since the nanofiber membrane is arrayed in the proposed device, the stiffness contrast between the membrane and the frame areas is extremely high. Furthermore, the stiffness of the nanofiber membrane might not be homogenous. Based on the plate theory [63], the radial and tangential strains of a membrane with 100 μm center deflection were plotted (Fig. S1B). Clearly, the radial strain is maximum at r ~ 0.6R and the tangential strain is minimum at r ~ 0.8R, where r is the distance from the center and R is the radius of membrane.

3.2 Guided self-organization of neural networks

NPCs were derived from hiPSCs by using a commonly used protocol [5] (Fig. 2A). The derived NPCs could be passaged for expansion, cryopreserved, and differentiated into different types of neural cells. As shown in Fig. S2A, hiPSCs colonies (D0) were detached to form embryoid bodies (EBs) in ultra-low attachment wells on day 2. After being cultured in the neural induction medium (NIM) for 3 days, larger EBs with smooth edges (day 5) were generated and gave rise to spread cell sheet after transferring them on a laminin-coated tissue culture plate from day 6 to day 15. On day 40, homogenous NPCs were obtained. The proliferation of NPCs was shown in Fig. S2B after 5 passages. At this stage, cells were stained with a neuronal progenitor marker, Nestin (red), and neuron-specific cytoskeleton marker, β-III tubulin (TUJ 1, green), showing that all cells expressed Nestin, whereas only a part of the cells co-expressed TUJ 1 (Fig. S2C and S2D). As a development signature of the NPCs, neural rosettes could be observed (Figure S2C and S2D). Meanwhile, NPCs of different nuclei sizes in the center and around of the neural rosettes were found, indicating the diversity of the NPC types (Figure S2D, zoomed image).

Clearly, the distribution of the differentiated NPCs changes with culture time until day 56 and depends on the type of substrates. After differentiation for 56 days, cell clusters were found in all honeycomb compartments of the patch, due to the stiffness and permeability modulation of the substrate (Fig. 2B-C). On the nanofiber covered-glass, cells were likely uniformly distributed due to the cell retention effects of nanofibers (Fig. 2C, middle). On the glass substrate, small and large clusters with stretched radial neurites appeared (Fig.2C, right). More importantly, we found that the neural clusters poorly adhered on the glass substrate and can be easily detached in the

end during the culture medium exchange, whereas they robustly remained on the nanofiber-covered glass and the patch. Thus, this strong interaction between cells and nanofiber-type substrates makes the possibility for the long-term neural culture *in vitro*.

A more detailed observation suggested that the nanofibers promoted cell adhesion (Fig. S3; days 1 and 3). From day 3 to day 12, neural clusters underwent both neurogenesis and gliogenesis. On the arrayed monolayer nanofibers, neural cells firstly aggregated in both areas of the membrane and the frame and then migrated into the membrane area, leaving a limited number of cells but a large number of neurites on the frame (Fig. S3, day 12). The cell distribution of the NPCs on days 3 and 56 after seeding was reported in Figure 2D-E, which clearly shows that the cells tended to aggregate in the center of the honeycomb compartment and formed a quasi-3D cluster of ~ 30 μm height and ~ 549 ± 101 cells on day 56.

Fig. 2F and S4A show the immunofluorescence images of the neural clusters on the three types of substrates after differentiation for 56 or 70 days. Cell nuclei were labeled by DAPI (blue), dendrites were labeled by microtubule-associated protein 2 (MAP2, green), and the identified clusters were indicated by red lines (see method). Interestingly, cell nuclei were mostly located in the center of the membrane areas of honeycomb compartments on the arrayed nanofiber membrane. Remarkably, only a few nuclei were found in the frame areas and the clusters were inter-connected by stretched dendrite bundles. The organization of the cluster and stretched radial neurites on the glass slide can now be more clearly seen. Meanwhile, we found that cells were organized into small clusters quite homogenously and inter-connected on the nanofiber-covered glass substrate. More detailed analyses allowed us to determine the nuclei (DAPI) and dendrite (MAP2) density of clusters, cluster size, and the inter-cluster distance on different types of substrates, as shown in Fig. 2G-I. From these plots, we can see that both nuclei and dendrites in the cluster areas on the two nanofiber types of substrates are comparable. The density of nuclei and dendrites inside the neural clusters on the patch is significantly higher than that on nanofiber-glass. Besides, the size of the neural clusters on the nanofiber membrane (~ 24000 μm^2) is significantly larger than that on nanofiber covered glass (~ 4300 um^2) but smaller than that on glass (Figure 2C, 2F and S4A). As expected, the inter-cluster distance of the clusters on the nanofiber-glass and glass slide varied but it was well-defined on the arrayed nanofiber membrane.

3.3 Distribution and expression of neurons and glial cells

Neurons and glial cells were analyzed by cell staining with neurofilament 200 (red), GFAP (green) and DAPI (blue) after differentiation for 56 days. In Fig. 3A, interconnected-clusters with remarkable axons outgrowth (white arrows) perpendicular to the edge of the hexagonal structure are shown. Multipolar neurons with different soma morphology including pyramidal-like neurons could be observed (Fig. 3B, cyan arrows). The differences in distribution and expression of neurons and glial cells on two types of substrates can be seen in Fig. 3C. Remarkably, a low percentage of astrocytes were found on the nanofiber-membrane than that on nanofiber-covered glass (Fig. 3C, 3E, top) but the expression-level of the neurons on two types of substrates are comparable (Fig. 3E bottom). The glia-neuron ratio of neural networks at day 56 on nanofiber membrane, nanofiber-covered glass and glass are ~0.29, ~0.5 and ~0.71, respectively. These differences could result from the varied culture materials, stiffness and permeability of the substrates. Different phenotypes of astrocyte-like glial cells could also be observed (Fig. 3D).

The cells were also labeled by MAP2 (green), GFAP (red), and DAPI (blue) for analyzing matured neurons and astrocytes (Fig. 3F). Now, the entanglement of glial cells inside the clusters can be more clearly seen. These neuron-astrocyte interactions are crucial for signaling and neural metabolism. As described before, cells spontaneously aggregated on the glass slide to form small and large clusters with long and stretched neurites. Here, we found that these neurites were organized to form bundles and that dense bundles of GFAP+ astrocytes superimposed on some the neurons. These GFAP+ bundles could provide a strong support for the extension of other neurites. In contrast, few stretch bundles were observed in the neural networks on neither nanofiber-covered glass nor nanofiber membrane.

3.4 Glucose-sensing neurons

To demonstrate the existence of glucose-sensing neurons in our neural network, we analyzed the calcium transient without and with 10 mM glucose. Neural networks that differentiated on a nanofiber membrane for 189 days were used to study. We found that only a few cells became exciting after the glucose addition. The cells which are glucose-sensitive increased the frequency of the calcium transient (Fig. 3G). The calcium influx also significantly increased by reflecting with the fluorescent density

amplification. Interestingly, ROI 1 and 2 in the neural cluster were in synchrony before and after the glucose addition. The maturity and functionality of the neural networks which developed on the nanofiber membrane were proved. By this experiment, we indirectly indicated the practicability of this neural system for chemical stimulation research at the same time.

3.5 Enhanced neural activity by guided neural clusters

Fluo-4 acetoxymethyl ester (Fluo-4 AM) was used as an indicator to monitor Ca^{2+} waves of differentiating neural networks formed on the three types of substrates. Ca^{2+} wave images were recorded. Fig. S5 illustrates typical calcium transient images of the neural networks after NPCs differentiation for 56 days and neural signals extracted from these images. Red contours indicated region of interest (ROIs). ΔF/F traces of representative ROIs were classified in different colors based on the frequency of the signals. As can be seen, the neural networks on the nanofiber membrane are more active than those on glass or nanofiber-covered glass, due to guided self-differentiation of neural clusters (Fig. S5). However, no synchronized neural activity has been observed, due probably to the poor or unstable synaptic connections, as discussed below.

3.6 Automated differentiation of NPCs toward neural networks

To improve the performance of neural differentiation of NPCs, an automated culture system was developed for long-term operation without manual intervention (Fig. 4A-4C). For comparison, manual differentiation was also conducted and both were performed with arrayed nanofiber membranes. In Fig. S6A, the phase contrast images of NPCs on days 14, 36, 52 and 62 are shown, indicating that in both cases of automated and manual differentiation cells migrated to the center area of the honeycomb compartment to form large clusters with radial outgrowth of neural cells. To evaluate the performance of the process, the cells on day 78 were labeled with synapsin I (green) and Tau (red), which respectively show the distribution of synaptic vesicle proteins and neural axons. Fig. 4D and S6B show entangled axons along with synapsin I in two areas inside the cluster. Remarkably, dense synaptic spots along the axons are observed in automatically differentiated network but much less can be seen in manually differentiated one. Quantitatively, about 2-fold increase in synaptic spot size, 3-fold increase in synaptic spot number and 1.5-fold increase in integrated

fluorescence density of synapsin I inside the neural clusters were deduced comparing the automatically derived network to the manually derived one (Fig. 4F, 4G). In contrast, a comparable expression-level of Tau protein can be noticed found, suggesting a comparable number of axons (Fig. 4D, 4G). MAP2 labeled dendrites in the derived neural networks are also shown (Fig. 4E), indicating that in both cases the nuclei density is high in the center of the honeycomb compartment and the expression levels of MAP2 have no significant difference (Fig. 4G). Together, these findings indicated an increased number of the presynaptic protein synapsin I which provides presynaptic assembly [64], demonstrating unambitiously the advantage of the automatic method.

3.7 Synchronized activities of automatically derived neural networks

The neural activities in synchrony are crucial to the study of neural signal transmission, which are also a clear signature of network maturation. Our results showed that no synchronous activity appeared after manual differentiation for 56 days. A small group of synchronized signals could be detected after a longer period of maturation, but they were not significant for more detailed analyses. In contrast, automatic differentiation led systematically to synchronized neural activities. Fig. 5 shows a close comparison of the results obtained after manual and automatic differentiation for 78 days and analyzed by FluoroSNNAP [58]. 48 and 31 ROIs were respectively identified from Calcium image sequences recorded with the samples manually and automatically processed. Clearly, the automatically differentiated neural network showed more important and synchronized activities than that of the manual one. Global and partial signal synchronization (blue and yellow shades) could be identified inside the neural networks generated automatically. Furthermore, the neural activities in some of the ROIs are not only synchronized, but also have additional calcium transients (ROI 5, 12, 22 and 25). Knowing that the displayed image was entirely inside a honeycomb compartment and many radial neurites crossing the frame were observed (Fig. S7), the additional peaks of these ROIs might be related to the neural activities of the neighboring clusters. Thus, they may play the role of connector hubs [65] and contribute to both segregated and global “processing” [66], suggesting that it would be possible to develop a higher degree of synchronous neural activities. The raster plot graphs in Fig. 5C summarize the calcium events showing more clearly

the differences between dispersed and synchronized neural signals of manually and automatically differentiated networks. Altogether, a better neural connectivity was found in the clusters of automatically differentiated network than that of manual one, demonstrating the advantage of automatic medium replacement for long-term neural differentiation.

4. Discussion

Human brain cortex is an extraordinary soft tissue (<1 kPa) [67] with a stiffness much smaller than most of other tissue types [61]. Such a soft stiffness is a biophysical effector in neural network development and neural function implementation *in vitro* [68-70]. Here, we developed a controllable cluster neural network derived from hiPSCs on nanofibrous membrane. The nanofiber membrane composed arrayed honeycomb frame and crosslinked gelatin nanofiber provides a low stiffness array. Accordingly, the permeability of the device was also arrayed, giving rise to a planar culture substrate with high contrast modulation of both stiffness and permeability. On our arrayed nanofiber membrane, the low stiffness coupled with the high permeability results in hiPSCs-derived NPCs accumulation, differentiation and generation of arrayed inter-connected clusters. Such an extremely substrate induced cell self-organization, clustering orderly, neuron enrichment, cortical neural network maturation and maintainment by comparison with two other types of substrates (glass and nanofiber covered glass) after monthly differentiation. It fully displays the advantages of this ECM-like gelatin nanofiber, including soft stiffness, nanoscale structure and biocompatibility.

Human brain cortex is composed of large populations of glia and neurons and the glia-neuron ratio is varied in the different human cortical regions between 1-3 and shows a fundamental effect on brain functions [71]. Glia cells regulate the levels of substances that neurons need in the intercellular space, provide a structural framework for neurons and isolate them so they can conduct electrical signals more efficiently. Neurons are key cells for understanding how the brain works. Interestingly, significant neuron-glia interaction and enhanced signal propagations inside the neural clusters were observed on the nanofiber membrane, although the proportion of glial cells was not high by comparison with in vivo. To increase the glia-neuron ratio, the component, density or diameter of nanofibers can be altered to obtain different mechanical properties or bioactivities properties of the nanofiber membrane. As reported [70,72,73], these aspects (the component, density or diameter of nanofibers) have great impacts on guiding cell fate during neural differentiation. In addition, a vary glia-neuron ratio can also gained by regulating the cell differentiation signal by factors such as ciliary neurotrophic factor [74]. What cannot be ignored is that the brain has evolved characteristically in the brain structure, changes in gene expression, and cell populations and ratios. These characteristics are essential for the performance of higher functions, such as sociality, language, and cognition, that express humanity, and are thought to have been acquired over evolutionary time. The impact of astrocyte and microglia activity on behavioral

outcomes for higher and finer control, for example higher cognitive control, reward-seeking, and circadian regulation, may explain a sharply increased glia-neuron ratio in primates. Maybe pursuing the final ratio is not the aim, but to build a network of neurons with effective reactivity.

The emergence and evolution of synchronized clusters are both important for cortical network functions. The neuronal synchronization is due to interactions between neurons via synaptic coupling and phase locking between a group of neurons, which can be understood theoretically [75]. While local synchronization can be studied by Ca^{2+} transient wave analyses, long-range synchronization can be more easily monitored by extracellular potential recording by using multielectrode array (MEA) techniques. In both cases, new methods and new tools of controlling cluster formation are needed to enable a more systematic investigation of network functions. In this regard, the arrayed nanofiber membrane has inherent advantages for the network designing and monitoring [49] by comparison randomly neural networks formation in vitro [76-78]. Additionally, the arrayed nanofiber membrane is capable for co-culture studies and in vitro modelling by coupling with brain endothelial cells and/or immune cells (i.e., microglia cells) on another side of the nanofiber membrane. Moreover, the vertical culture space of nanofiber membrane can be expanded by gel embedding for guiding spatial polarization of NPCs with longitudinal mechanical force to generate in-vivo like cortical architecture.

Automation of hiPSCs-derived neuron differentiation have been shown in a plenty of advantages in terms of long-term culture, consistency and accuracy maintainment and reducing labor [79-81]. Automated methods contributed to more effective research into neurodegenerative diseases, including Alzheimer's disease and Parkinson's disease [80,81]. Here, we showed that automatic differentiation promotes synaptic expression and assembling, enabling synchronous neural activities of the network in comparison to the manual differentiation method on the nanofiber membrane. More accurate and standard manipulation, less operational distractions and temperature variation may contribute to these improved neural networks formation. Our automated system performed an outstanding stability and reliability in charge of the challenge of long-term differentiation and reducing risks of misoperation and contamination like other platforms. However, it is affordable for research and small-scale development by comparison to the large automated systems do exist for mass production [79-83]. Because the protocol for generation of cortical neural networks here is relatively simple involving only one type in the final differentiation and maturation step. And hiPSCs-derived neural precursor cells (NPCs) are easy to obtain and can directly differentiate into cortical neural networks since NPCs can be expanded, cryopreserved, and used for many times. Thus, this dedicated system including one medium bottom and six culture dishes, is particularly designed and suited for automation of long-term processing such as differentiation of neural precursor cells (NPCs) toward cortical neural networks. The combination of this simple cortical neuron network differentiation protocol and automation techniques is effective and promising for further human brain studies. What's more, this automated system is versatile and flexible to reassemble or reprogram to meet the new culture conditions, differentiation

protocols or drug screening. An example was showed a different system involved six types of culture media but only one culture ware for automated differentiation of hiPSCs toward cardiomyocytes [57]. A fluid culture system can be easily set up by system programming for dynamic culture and an electrical stimulation unit can be integrated in the culture system. To integrate an automated real-time image monitoring unit is also benefits for this long-term differentiation process.

We would like to mention that the present work is a proof-of-concept with only one device configuration. By varying the geometric parameters of the honeycomb microframe, the array, shape and size of the honeycomb frame on the nanofiber membrane can be easily changed by lithography method [51, 52]. The distribution, shape, size of clusters and inter-connections between clusters can be altered. This would allow creation of different scales of neural networks for functional studies. Furthermore, the differentiated neural networks can also be integrated into microfluidic devices for organ-on-a-chip studies. electric, chemical, and other types of stimuli can be applied to detect the response and evolution of the networks. Finally, this approach can be extended to neural disease modeling, brain-computer interface studies and drug screening.

Declaration of competing interest

No.

Acknowledgement

B. H. has been supported by a Guangzhou Elite Fellowship. This work has been supported by grants from Agence Nationale pour la Recherche (ANR-17-CE09-0017 and ANR-19-CE18-0009-01), Région Ile-de-France (DIM-ELICIT), PSL-valorization (program pre-maturation), Carnot IPGG, and European Commission Cost Action BIONECA (CA 16122).

References

[1] K. Takahashi, K. Tanabe, M. Ohnuki, M. Narita, T. Ichisaka, K. Tomoda, S. Yamanaka, Induction of Pluripotent Stem Cells from Adult Human Fibroblasts by Defined Factors, Cell. 131 (2007) 861-872. https://doi.org/10.1016/j.cell.2007.11.019.

[2] M.A. Lancaster, M. Renner, C.A. Martin, D. Wenzel, L.S. Bicknell, M.E. Hurles, T. Homfray, J.M. Penninger, A.P. Jackson, J.A. Knoblich, Cerebral organoids model human brain development and microcephaly, Nature. 501 (2013) 373-379. https://doi.org/10.1038/nature12517.

[3] S. Velasco, A.J. Kedaigle, S.K. Simmons, A. Nash, M. Rocha, G. Quadrato, B. Paulsen, L. Nguyen, X. Adiconis, A. Regev, J.Z. Levin, P. Arlotta, Individual brain organoids reproducibly form cell diversity of the human cerebral cortex, Nature. 570 (2019) 523-527. https://doi.org/10.1038/s41586-019-1289-x.

[4] Y. Shi, P. Kirwan, F.J. Livesey, Directed differentiation of human pluripotent stem cells to cerebral cortex neurons and neural networks, Nature Protocols. 7 (2012) 1836-1846. https://doi.org/0.1038/nprot.2012.116.

[5] N. Gunhanlar, G. Shpak, M. van der Kroeg, L.A. Gouty-Colomer, S.T. Munshi, B. Lendemeijer, M. Ghazvini, C. Dupont, W.J.G. Hoogendijk, J. Gribnau, F.M.S. de Vrij, S.A. Kushner, A simplified protocol for differentiation of electrophysiologically mature neuronal networks from human induced pluripotent stem cells, Mol Psychiatry. 23 (2018) 1336-1344. https://doi.org/10.1038/mp.2017.56.

[6] Y.J. Hong, J.T. Do, Neural Lineage Differentiation From Pluripotent Stem Cells to Mimic Human Brain Tissues, Front Bioeng and Biotechnol. 7 (2019) 400. https://doi.org/10.3389/fbioe.2019.00400.

[7] Bassett DS, Sporns O. Network neuroscience, Nat Neurosci. 20 (2017) 353-364. https://doi.org/10.1038/nn.4502.

[8] M. Lodi, F.D. Rossa, F. Sorrentino, M. Storace, Analyzing synchronized clusters in neuron networks, Sci Rep. 10 (2020) 16336. https://doi.org/10.1038/s41598-020-73269-9.

[9] M. Chiappalone, A. Vato, L. Berdondini, M. Koudelka-Hep, S. Martinoia. Network dynamics and synchronous activity in cultured cortical neurons, Int J Neural Syst. 17 (2007) 87-103. https://doi.org/10.1142/S0129065707000968

[10] M.S. Schroeter, P. Charlesworth, M.G. Kitzbichler, O. Paulsen, E.T. Bullmore, Emergence of rich-club topology and coordinated dynamics in development of hippocampal functional networks in vitro, J Neurosci. 35 (2015) 5459-5470. https://doi.org/10.1523/JNEUROSCI.4259-14.2015.

[11] J. Izsak, H. Seth, M. Andersson, D. Vizlin-Hodzic, S. Theiss, E. Hanse, H. Ågren, K. Funa, S. Illes, Robust Generation of Person-Specific, Synchronously Active Neuronal Networks Using Purely Isogenic Human iPSC-3D Neural Aggregate Cultures, Front Neurosci. 24 (2019) 351. https://doi.org/10.3389/fnins.2019.00351.

[12] I. Shoko, S. Kenta, S. Koji, K. Kiyoshi, J. Yasuhiko, Synchronous firing patterns of induced pluripotent stem cell-derived cortical neurons depend on the network structure consisting of excitatory and inhibitory neurons, Biochem Biophys Res Commun. 501(2018)152-157. https://doi.org/10.1016/j.bbrc.2018.04.197.

[13] M.M. Adil, A.T. Rao, G.N. Ramadoss, N.E. Chernavsky, R.U. Kulkarni, E.W. Miller, S. Kumar, D.V. Schaffer, Dopaminergic Neurons Transplanted Using Cell-Instructive Biomaterials Alleviate Parkinsonism in Rodents, Adv Func Mater. 28 (2018) 1804144. https://doi.org/10.1002/adfm.201804144.

[14] S.M. Ojovan, M. McDonald, N. Rabieh, N. Shmuel, H. Erez, M. Nesladek, M.E. Spira, Nanocrystalline diamond surfaces for adhesion and growth of primary neurons, conflicting results and rational explanation, Front Neuroeng. 7 (2014) 17. https://doi.org/10.3389/fneng.2014.00017.

[15] N. Arimura, K. Kaibuchi, Neuronal polarity: from extracellular signals to intracellular mechanisms, Nat Rev Neuro. 8 (2007) 194-205. https://doi.org/10.1038/nrn2056.

[16] H. Sakaguchi, Y. Ozaki, T. Ashida, T. Matsubara, N. Oishi, S. Kihara, J. Takahashi, Self-Organized Synchronous Calcium Transients in a Cultured Human Neural Network Derived from Cerebral Organoids, Stem Cell Reports. 13 (2019) 458-473. https://doi.org/10.1016/j.stemcr.2019.05.029.

[17] T. Sato, K. Imaizumi, H. Watanabe, M. Ishikawa, H. Okano, Generation of region-specific and high-purity neurons from human feeder-free iPSCs, Neurosci Lett. 16 (2021) 135676. https://doi.org/10.1016/j.neulet.2021.135676.

[18] A. Odawara, H. Katoh, N. Matsuda, I. Suzuki, Physiological maturation and drug responses of human induced pluripotent stem cell-derived cortical neuronal networks in long-term culture, Sci Rep. 6 (2016) 26181. https://doi.org/10.1038/srep26181.

[19] M.A. Lancaster, N.S. Corsini, S. Wolfinger, E.H. Gustafson, A.W. Phillips, T.R. Burkard, T. Otani, F.J. Livesey, J.A. Knoblich, Guided self-organization and cortical plate formation in human brain organoids, Nat Biotechnol. 35 (2017) 659-666. https://doi.org/10.1038/nbt.3906.

[20] E. Karzbrun, A. Kshirsagar, S.R. Cohen, J.H. Hanna, O. Reiner, Human brain organoids on a chip reveal the physics of folding, Nat Phys. 14 (2018) 515-522. https://doi.org/10.1038/s41567-018-0046-7.

[21] A. Chen, Z. Guo, L. Fang, S. Bian, Application of Fused Organoid Models to Study Human Brain Development and Neural Disorders, Front Cell Neurosci. 14 (2020) 133. https://doi.org/10.3389/fncel.2020.00133.

[22] G. Quadrato, P. Arlotta, Present and future of modeling human brain development in 3D organoids, Current Opinion in Cell Biology. 49 (2017) 47-52. https://doi.org/10.1016/j.ceb.2017.11.010.

[23] R. Rauti, N. Renous, B.M. Maoz, Mimicking the Brain Extracellular Matrix in Vitro: A Review of Current Methodologies and Challenges, Isr J Chem. 60 (2020) 1141-1151. https://doi.org/10.1002/ijch.201900052.

[24] N.D. Leipzig, M.S. Shoichet, The effect of substrate stiffness on adult neural stem cell behavior, Biomaterials. 30 (2009) 6867-6878. https://doi.org/10.1016/j.biomaterials.2009.09.002

[25] S. Musah, P.J. Wrighton, Y. Zaltsman, X. Zhong, S. Zorn, M.B. Parlato, C. Hsiao, S.P. Palecek, Q. Chang, W.L. Murphy, L.L. Kiessling, Substratum-induced differentiation of human pluripotent stem cells reveals the coactivator YAP is a potent regulator of neuronal specification, Proc Natl Acad Sci USA. 111 (2014) 13805-13810. https://doi.org/10.1073/pnas.1415330111.

[26] T. Hyvärinen, A. Hyysalo, F.E. Kapucu, L. Aarnos, A. Vinogradov, S.J. Eglen, L. Ylä-Outinen, S. Narkilahti, Functional characterization of human pluripotent stem cell-derived cortical networks differentiated on laminin-521 substrate: comparison to rat cortical cultures, Sci Rep. 9 (2019) 17125. https://doi.org/10.1038/s41598-019-53647-8.

[27] Z.N. Zhang, B.C. Freitas, H. Qian, J. Lux, A. Acab, C.A. Trujillo, R.H. Herai, V.A. Nguyen Huu, J.H. Wen, S. Joshi-Barr, J.V. Karpiak, A.J. Engler, X.-D. Fu, A.R. Muotri, A. Almutairi, Layered hydrogels accelerate iPSC-derived neuronal maturation and reveal migration defects caused by MeCP2 dysfunction, Proc Natl Acad Sci USA. 113 (2016) 3185-3190. https://doi.org/10.1073/pnas.1521255113.

[28] U.A. Aregueta-Robles, P.J. Martens, L.A. Poole-Warren, R.A. Green. Tissue engineered hydrogels supporting 3D neural networks. Acta Biomater. 95 (2019) 269-284. doi: 10.1016/j.actbio.2018.11.044.

[29] Y. Zhu, L. Wang, H. Yu, F. Yin, Y. Wang, H. Liu, L. Jiang, J. Qin, In situ generation of human brain organoids on a micropillar array, Lab Chip. 17 (2017) 2941-2950. https://doi.org/10.1039/C7LC00682A.

[30] A. Cutarelli, S. Ghio, J. Zasso, A. Speccher, G. Scarduelli, M. Roccuzzo, M. Crivellari, N. Maria Pugno, S. Casarosa, M. Boscardin, L. Conti, Vertically-Aligned Functionalized Silicon Micropillars for 3D Culture of Human Pluripotent Stem Cell-Derived Cortical Progenitors, Cells. 9 (2019) 88. https://doi.org/10.3390/cells9010088.

[31] A. Chen, X. Dong, K.-H. Fang, F. Yuan, Y. Hu, M. Xu, Y. Huang, X. Zhang, D. Fang, Y. Liu, Develop a 3D neurological disease model of human cortical glutamatergic neurons using micropillar-based scaffolds, Acta Pharm Sin B. 9 (2019) 557-564. https://doi.org/10.1016/j.apsb.2019.03.004

[32] J. Xie, M.R. MacEwan, A.G. Schwartz, Y. Xia, Electrospun nanofibers for neural tissue engineering, Nanoscale. 2(1) (2010) 35-44. https://doi.org/10.1039/B9NR00243J.

[33] S.H. Lim, X.Y. Liu, H. Song, K.J. Yarema, H.-Q. Mao, The effect of nanofiber-guided cell alignment on the preferential differentiation of neural stem cells, Biomaterials. 31(34) (2010) 9031-9039. https://doi.org/10.1016/j.biomaterials.2010.08.021.

[34] J. Wei, D. Pozzi, F.P. Ulloa Severino, V. Torre, Y. Chen, Fabrication of PLGA nanofibers on PDMS micropillars for neuron culture studies, Microelectronic Engineering. 175 (2017) 67-72. https://doi.org/10.1016/j.mee.2017.01.015.

[35] L. Song, K. Wang, Y. Li, Y. Yang, Nanotopography promoted neuronal differentiation of human induced pluripotent stem cells, Colloids Surf B Biointerfaces. 148 (2016) 49-58. https://doi.org/10.1016/j.colsurfb.2016.08.041.

[36] F. Pan, M. Zhang, G. Wu, Y. Lai, B. Greber, H.R. Schöler, L. Chi, Topographic effect on human induced pluripotent stem cells differentiation towards neuronal lineage, Biomaterials. 34 (2013) 8131-8139. https://doi.org/10.1016/j.biomaterials.2013.07.025.

[37] C. Luo, L. Liu, X. Ni, L. Wang, S. Nomura, Q. Ouyang, Y. Chen, Differentiating stem cells on patterned substrates for neural network formation, Microelectronic Engineering. 88 (2011) 1707-1710. https://doi.org/10.1016/J.MEE.2010.12.062.

[38] S. Ankam, M. Suryana, L.Y. Chan, A.A. Moe, B.K. Teo, J.B. Law, M.P. Sheetz, H.Y. Low, E.K. Yim. Substrate topography and size determine the fate of human embryonic stem cells to neuronal or glial lineage. Acta Biomater. 9 (2013) 4535-45. doi: 10.1016/j.actbio.2012.08.018.

[39] S. Bang, K.S. Hwang, S. Jeong, J.J. Cho, N. Choi, J. Kim, H.N/ Kim, Engineered neural circuits for modeling brain physiology and neuropathology. Acta Biomater. 132 (2021) 379-400. doi: 10.1016/j.actbio.2021.06.024.

[40] Z. Hesari, M. Soleimani, F. Atyabi, M. Sharifdini, S. Nadri, M.E. Warkiani, M. Zare, R. Dinarvand, A hybrid microfluidic system for regulation of neural differentiation in induced pluripotent stem cells, J Biomed Mater Res A. 104 (2016) 1534-1543. https://doi.org/10.1002/jbm.a.35689.

[41] C. Li, M. Kuss, Y. Kong, F. Nie, X. Liu, B. Liu, A. Dunaevsky, P. Fayad, B. Duan, X. Li, 3D Printed Hydrogels with Aligned Microchannels to Guide Neural Stem Cell Migration, ACS Biomater Sci Eng. 7 (2021) 690-700. https://doi.org/10.1021/acsbiomaterials.0c01619.

[42] T. Kirihara, Z. Luo, S.Y.A. Chow, R. Misawa, J. Kawada, S. Shibata, F. Khoyratee, C.A. Vollette, V. Volz, T. Levi, T. Fujii, Y. Ikeuchi, A Human Induced Pluripotent Stem Cell-Derived Tissue Model of a Cerebral Tract Connecting Two Cortical Regions, iScience. 14 (2019) 301-311. https://doi.org/10.1016/j.isci.2019.03.012.

[43] Smith, M. Haag, C. Ugbode, D. Tams, M. Rattray, S. Przyborski, A. Bithell, B.J. Whalley, Neuronal-glial populations form functional networks in a biocompatible 3D scaffold, Neurosci Lett. 609 (2015) 198-202. https://doi.org/10.1016/j.neulet.2015.10.044.

[44] F.P. Ulloa Severino, J. Ban, Q. Song, M. Tang, G. Bianconi, G. Cheng, V. Torre, The role of dimensionality in neuronal network dynamics, Sci Rep. 6 (2016) 29640. https://doi.org/10.1038/srep29640.

[45] S. Li, F.P.U. Severino, J. Ban, L. Wang, G. Pinato, V. Torre, Y. Chen, Improved neuron culture using scaffolds made of three-dimensional PDMS micro-lattices, Biomed Mater. 13 (2018) 034105. https://doi.org/10.1088/1748-605x/aaa777.

[46] E.G.Z. Centeno, H. Cimarosti, A. Bithell, 2D versus 3D human induced pluripotent stem cell-derived cultures for neurodegenerative disease modelling, Mol neurodegener. 13 (2018) 27-27. https://doi.org/10.1186/s13024-018-0258-4.

[47] S. Ortinau, J. Schmich, S. Block, A. Liedmann, L. Jonas, D.G. Weiss, C.A. Helm, A. Rolfs, M.J. Frech, Effect of 3D-scaffold formation on differentiation and survival in human neural progenitor cells, BioMed Eng Online. 9 (2010) 70. https://doi.org/10.1186/1475-925X-9-70.

[48] Y. Tang, L. Liu, J. Li, L. Yu, L. Wang, J. Shi, Y. Chen, Induction and differentiation of human induced pluripotent stem cells into functional cardiomyocytes on a compartmented monolayer of gelatin nanofibers, Nanoscale. 8 (2016) 14530-14540. https://doi.org/10.1039/C6NR04545F.

[49] Y. Tang, L. Liu, J. Li, L. Yu, F.P.U. Severino, L. Wang, J. Shi, X. Tu, V. Torre, Y. Chen, Effective motor neuron differentiation of hiPSCs on a patch made of crosslinked monolayer gelatin nanofibers, J of Mater Chem B. 4 (2016) 3305-3312. https://doi.org/10.1039/C6TB00351F.

[50] Y. Tang, F.P. Ulloa Severino, F. Iseppon, V. Torre, Y. Chen, Patch method for culture of primary hippocampal neurons, Microelectronic Engineering. 175 (2017) 61-66. https://doi.org/10.1016/j.mee.2017.01.012.

[51] B. Wang, L. Wang, Y. Tang, J. Shi, J. Wei, X. Tu, Y. Chen, Fabrication of spaced monolayers of electrospun nanofibers for three-dimensional cell infiltration and proliferation, Microelectronic Engineering. 198 (2018) 73-74. https://doi.org/10.1016/j.mee.2018.07.005.

[52] B. Huang, J. Peng, X. Huang, F. Liang, L. Wang, J. Shi, A. Yamada, Y. Chen, Generation of Interconnected Neural Clusters in Multiscale Scaffolds from Human-Induced Pluripotent Stem Cells, ACS Appl Mater Interfaces. 13 (2021) 55939-55952. https://doi.org/10.1021/acsami.1c18465.34788005.

[53] W. G. Gray and C. T. Miller, Examination of Darcy's Law for Flow in Porous Media with Variable Porosity, Environ Sci Technol. 38 (2004) 5895-5901. https://doi.org/10.1021/es049728w.

[54] F. Liang, X.C. Huang, J. Peng, H.Y. Luo, J. Shi, L. Wang, and Y. Chen, A microfluidic system for rapid determination of Darcy permeability of filtration membranes: from patterned micro-holes to artificial basement membranes, to be published

[55] M. Radiom, Y. He, J. Peng-Wang, A. Baeza-Squiban, J.F. Berret, Y. Chen, Alveolar mimics with periodic strain and its effect on the cell layer formation, Biotechnology and Bioengineering. 117 (2020) 2827. https://doi.org/10.1002/bit.27458.

[56] J. Schindelin, I. Arganda-Carreras, E. Frise, V. Kaynig, M. Longair, T. Pietzsch, S. Preibisch, C. Rueden, S. Saalfeld, B. Schmid, J. Y. Tinevez, D.J. White, V. Hartenstein, K. Eliceiri, P. Tomancak, A. Cardona, Fiji: an open-source platform for biological-image analysis, Nat Methods. 9 (2012) 676–682. https://doi.org/10.1038/nmeth.2019

[57] G. Pitingolo, Y. He, B. Huang, L. Wang, J. Shi, Y. Chen, An automatic cell culture platform for differentiation of human induced pluripotent stem cells, Microelectronic Engineering. 231 (2020) 111371. https://doi.org/10.1016/j.mee.2020.111371.

[58] T.P. Patel, K. Man, B.L. Firestein, D.F. Meaney. Automated quantification of neuronal networks and single-cell calcium dynamics using calcium imaging, J Neurosci Methods. 243 (2015) 26-38. https://doi.org/10.1016/j.jneumeth.2015.01.020.

[59] E. Rofaani, B. Huang, F. Liang, J. Peng and Y. Chen, Reconstituted basement membrane enables airway epithelium modeling and nanoparticle toxicity testing, Int J. Bio. Macromol., 204 (2022) 300-309, https://doi.org/10.1016/j.ijbiomac.2022.02.018

[60] E. Rofaani, Y. He, J. Peng and Y. Chen, Epithelial folding of alveolar cells derived from human induced pluripotent stem cells on artificial basement membrane. Acta Biomater. (2022). https://doi.org/10.1016/j.actbio.2022.03.022.

[61] C.F. Guimarães, L. Gasperini, A.P. Marques, R.L. Reis, The stiffness of living tissues and its implications for tissue engineering, Nat. Rev. Mater. 5 (2020) 351–370. https://doi.org/10.1038/s41578-019-0169-1.

[62] J.L. Gibson, M.F. Ashby, Cellular Solids: Structure and Properties, 2nd ed, Cambridge Univ. Press. (1997). https://doi.org/10.1017/CBO9781139878326.

[63] Y. Zhang, Large deflection of clamped circular plate and accuracy of its approximate analytical solutions. Science China Physics, Mechanics & Astronomy. 59 (2016), 624602. https://doi.org/10.1007/s11433-015-5751-y

[64] F.J. Mirza, S. Zahid, The Role of Synapsins in Neurological Disorders, Neurosci Bull. 34 (2018) 349-358. https://doi.org/10.1007/s12264-017-0201-7.

[65] E. Bullmore, O. Sporns, Complex brain networks: graph theoretical analysis of structural and functional systems, Nat Rev Neurosci. 10 (2009) 86–198. https://doi.org/10.1038/nrn2575.

[66] W.S. Gagan, Segregated Systems of Human Brain Networks, Trends Cogn Sci. 21 (2017) 981-996. https://doi.org/10.1016/j.tics.2017.09.006.

[67] S. Budday, T.C. Ovaert, G.A. Holzapfel, P. Steinmann, E. Kuhl, Fifty Shades of Brain: A Review on the Mechanical Testing and Modeling of Brain Tissue, Arch Comput Methods Eng. 27 (2020) 1187-1230. https://doi.org/10.1007/s11831-019-09352-w.

[68] S. Wu, R. Xu, B. Duan, P. Jiang, Three-Dimensional Hyaluronic Acid Hydrogel-Based Models for In Vitro Human iPSC-Derived NPC Culture and Differentiation, J Mater Chem B. 5 (2017) 3870-3878. https://doi.org/10.1039/C7TB00721C.

[69] S. K. Seidlits, Z. Z. Khaing, R. R. Petersen, J. D. Nickels, J. E. Vanscoy, J. B. Shear, C. E. Schmidt, The effects of hyaluronic acid hydrogels with tunable mechanical properties on neural progenitor cell differentiation, Biomaterials. 31 (2010) 3930–3940. https://doi.org/10.1016/j.biomaterials.2010.01.125.

[70] A. Farrukh, S. Zhao, A. del Campo, Microenvironments Designed to Support Growth and Function of Neuronal Cells, Front. Mater. 5 (2018) 62. https://doi: 10.3389/fmats.2018.00062.

[71] S. Herculano-Houzelm, The glia/neuron ratio: how it varies uniformly across brain structures and species and what that means for brain physiology and evolution, Glia. 62 (2014) 1377-1391. https://doi:10.1002/glia.22683.

[72] G.T. Christopherson, H. Song, H. Q. Mao, The influence of fiber diameter of electrospun substrates on neural stem cell differentiation and proliferation, Biomaterials. 30 (2008) 556–564. https://doi.org/10.1016/j.biomaterials.2008.10.004.

[73] M. C. Amores de Sousa, C. Rodrigues, I. Ferreira, M.M. Diogo, R. J. Linhardt, J. Cabral, F. C. Ferreira, Functionalization of Electrospun Nanofibers and Fiber Alignment Enhance Neural Stem Cell Proliferation and Neuronal Differentiation, Front Bioeng Biotechnol. 8 (2020) 580135. https://doi.org/10.3389/fbioe.2020.580135.

[74] N. Lee, M. K. Batt, B. A. Cronier, M. C. Jackson, J. L. Bruno Garza, D. S. Trinh, C. O. Mason, R. P. Spearry, S. Bhattacharya, R. Robitz, M. Nakafuku, A. J. MacLennan, Ciliary neurotrophic factor receptor regulation of adult forebrain neurogenesis, J Neurosci. 33 (2013) 1241–1258. https://doi.org/10.1523/JNEUROSCI.3386-12.2013.

[75] Y. Kuramoto, Chemical Oscillations, Waves, and Turbulence. New York, NY: Springer-Verlag, (1984).

[76] J. zsak, H. Seth, M. Andersson, D. Vizlin-Hodzic, S. Theiss, E. Hanse, H. Agren, K. Funa, S. Illes, Robust Generation of Person-Specific, Synchronously Active Neuronal Networks Using Purely

Isogenic Human iPSC-3D Neural Aggregate Cultures, Front Neurosci.13 (2019) 351. https://doi.org/10.3389/fnins.2019.00351.

[77] A. Koroleva, A. Deiwick, A. El-Tamer, L. Koch, Y. Shi, E. Estévez-Priego, A.A Ludl, J. Soriano, D. Guseva, E. Ponimaskin, B. Chichkov, In Vitro Development of Human iPSC-Derived Functional Neuronal Networks on Laser-Fabricated 3D Scaffolds. ACS Appl Mater Interfaces. 13(2021) 7839–7853. https://doi.org/10.1021/acsami.0c16616.

[78] T. Hyvärinen, A. Hyysalo, F.E. Kapucu, L. Aarnos, A. Vinogradov, S.J. Eglen, L. Ylä-Outinen, S. Narkilahti, Functional characterization of human pluripotent stem cell-derived cortical networks differentiated on laminin-521 substrate: comparison to rat cortical cultures. Sci Rep, 9 (2019) 17125. https://doi.org/10.1038/s41598-019-53647-8.

[79] A. Dhingra, J. Täger, E. Bressan, S. Rodriguez-Nieto, M.S. Bedi, S. Bröer, E. Sadikoglou, N. Fernandes, M. Castillo-Lizardo, P. Rizzu, P. Heutink, Automated Production of Human Induced Pluripotent Stem Cell-Derived Cortical and Dopaminergic Neurons with Integrated Live-Cell Monitoring, J Vis Exp, 162 (2020) e61525. https://doi.org/10.3791/61525.

[80] K.I.W. Kane, E.L. Moreno, S. Hachi, M. Walter, J. Jarazo, M. Oliveira, T. Hankemeier, P. Vulto, J.C. Schwamborn, M. Thoma, R. Fleming, Automated microfluidic cell culture of stem cell derived dopaminergic neurons, Sci Rep, 9 (2019) 1796. https://doi.org/10.1038/s41598-018-34828-3.

[81] R. Bassil, K.Shields, K. Granger, I. Zein, S. Ng, B. Chih, Improved modeling of human AD with an automated culturing platform for iPSC neurons, astrocytes and microglia, Nat Commun, 12 (2021) 5220. https://doi.org/10.1038/s41467-021-25344-6.

[82] M. Serra, C. Brito, E.M. Costa, M.F.Q. Sousa, P.M. Alves, Integrating human stem cell expansion and neuronal differentiation in bioreactors, BMC Biotechnol. 9 (2009) 82. https://doi.org/10.1186/1472-6750-9-82.

[83] S. Konagaya, T. Ando, T. Yamauchi, H. Suemori, H. Iwata, Long-term maintenance of human induced pluripotent stem cells by automated cell culture system, Sci Rep. 5 (2015) 16647. https://doi.org/10.1038/srep16647.

Figure captions

Fig. 1. Culture device with an arrayed nanofiber membrane. A) Photograph of a device handled with a tweezer. B) Schematic illustration of the device consisting of a monolayer of crosslinked gelatin nanofibers on a patterned honeycomb microframe. C) SEM image of the nanofibers on the microframe. D) Percentages of small, middle, and large pore areas of the nanofiber membrane (n=3). E) Flowrate of DI water across a device with and without nanofibers. F) Cell number on different substrates before and after centrifugal force applied on cells (n=3). G) Young's modulus of the nanofiber membrane and two reference thin films.

Fig. 2. Formation of cortical neural network from hiPSCs. A) Stepwise differentiation protocol. B) Schematic illustration of cluster formation on a nanofiber membrane. C) Phase contrast images of NPCs on days 41 and 96. D) Top view and cross-sectional view of fluorescence image of the cell (DAPI) on days 43 and 96 on a nanofiber-membrane. E) Fluorescence intensity profiles of the image centerline and cluster height on days 43 and 96 (n=3). F) Immunofluorescence images of the neural network on day 96. Nuclei and dendrites were labeled by DAPI (blue) and MAP2 (green), respectively. Counters of the clusters were marked with red lines. Scale bars, 100 μm G) Averaged fluorescence intensity of DAPI and MAP2 of the clusters (n>3). H) Statistics of cluster area (n>3). I) Statistics of neighboring inter-cluster distance (n=3). P values were calculated by Student's t-test. *P < 0.05 and *** P < 0.001.

Fig. 3. Self-organized neural networks on different substrates. Cells were fixed after differentiation of NPCs 56 days. Neural axons, dendrites, glial cells, and cell nuclei were labeled by Neurofilament 200 (NF200), MAP2, GFAP, and DAPI, respectively. A) Large-scale view of interconnected clusters on an arrayed nanofiber-membrane. White arrows show interconnected axons perpendicular to the edge of the hexagonal structure. B-D) Clusters showing multiple neurons and glial cells. White and cyan arrows show two types of neurons identified by morphology. E) Bar graph of relative integrated density of GFAP and NF200 (n=3). P values were calculated by Student's t-test. **P < 0.01. F) Clusters showing entangled neurons and glial cells. Light blue hexagon indicates the edge of the honeycomb compartment. Scale bar, 100 μm. G) Neural signals of Ca^{2+} waves from the same neural network on nanofiber membrane with and without 10 mM D-glucose in the recording buffer.

Fig. 4. Automated differentiation and derived neural networks. A) Schematic timeline of manual and automated differentiation. B) Schematic diagram of an automated system with six culture dishes. C) Photograph of the automated system. From left to right: medium supply and waste, peristatic pump unit, and culture unit with six 60 mm diameter culture dishes and cover plates. D) Immunofluorescent images of the neural networks on day 78 stained to show synapses (Synapsin I, green), axons (Tau, red), and nuclei (DAPI, blue). Scale bars, 20 μm. E) Immunofluorescent images of the neural networks stained to show neurites (MAP2, red) and nuclei (DAPI, blue). Scale bars, 50 μm. F) Quantification of synaptic spots number and size (n = 3). G) Relative integrated density of Syn I, Tau, and MAP2 (n = 3).

Fig. 5. Neural activities of the clusters generated by manual and automated differentiation from NPCs for 78 days. A) Ca^{2+} images with ROIs. B) Neural signals ($\Delta F/F$) of the ROIs extracted from the Ca^{2+} images as a function of time. Global and partial signal correlations were marked by blue and yellow shades, respectively. C) Raster plots of the neural signals of the ROIs.

Fig.1

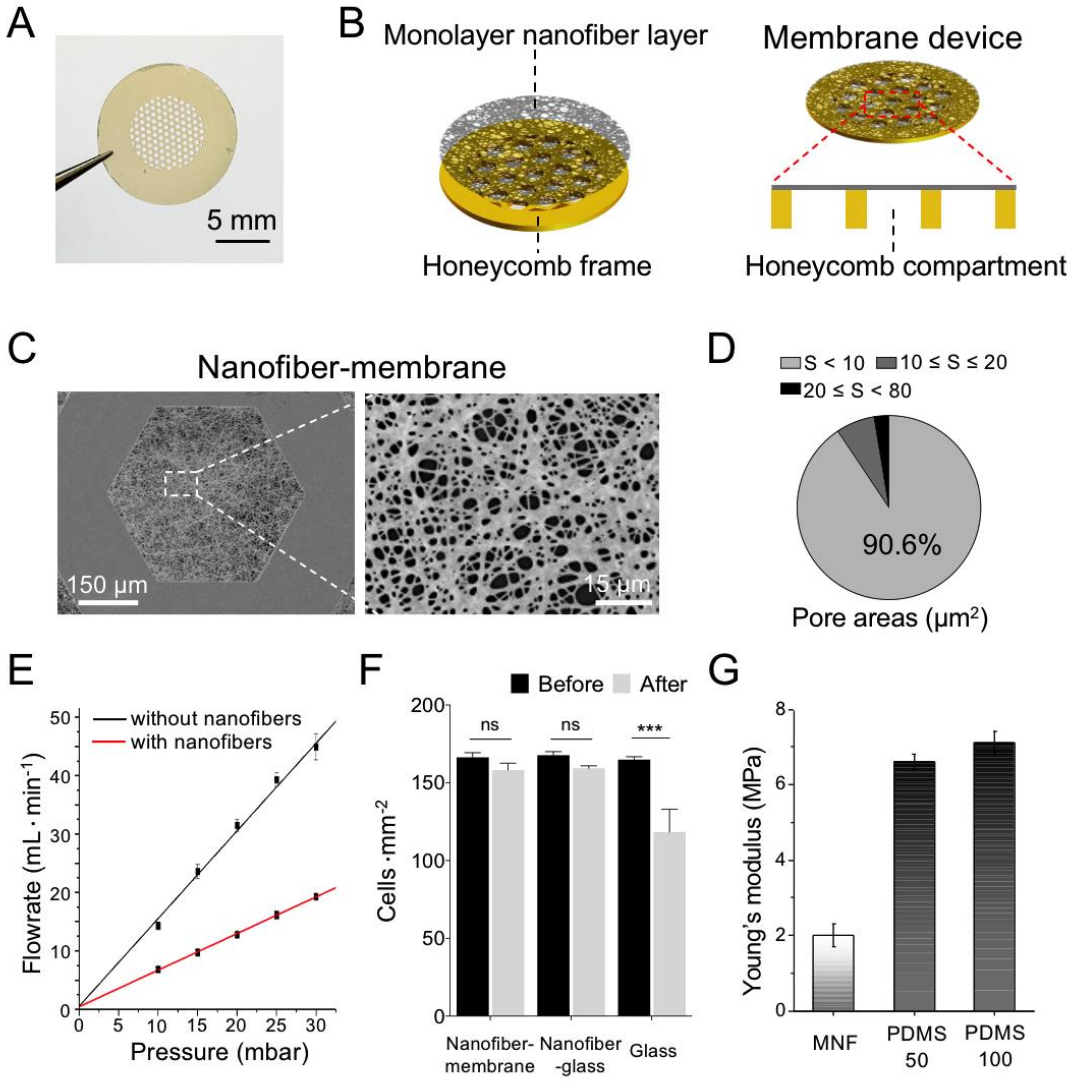
A
5 mm
B
Monolayer nanofiber layer
Membrane device
Honeycomb frame
Honeycomb compartment
C
Nanofiber-membrane
150 μm
15 μm
D
S < 10
10 ≤ S ≤ 20
20 ≤ S < 80
90.6%
Pore areas (μm²)
E
without nanofibers
with nanofibers
Flowrate (mL · min⁻¹)
Pressure (mbar)
F
Before
After
ns
ns
***
Cells ·mm⁻²
Nanofiber-membrane
Nanofiber-glass
Glass
G
Young's modulus (MPa)
MNF
PDMS 50
PDMS 100

Fig.2

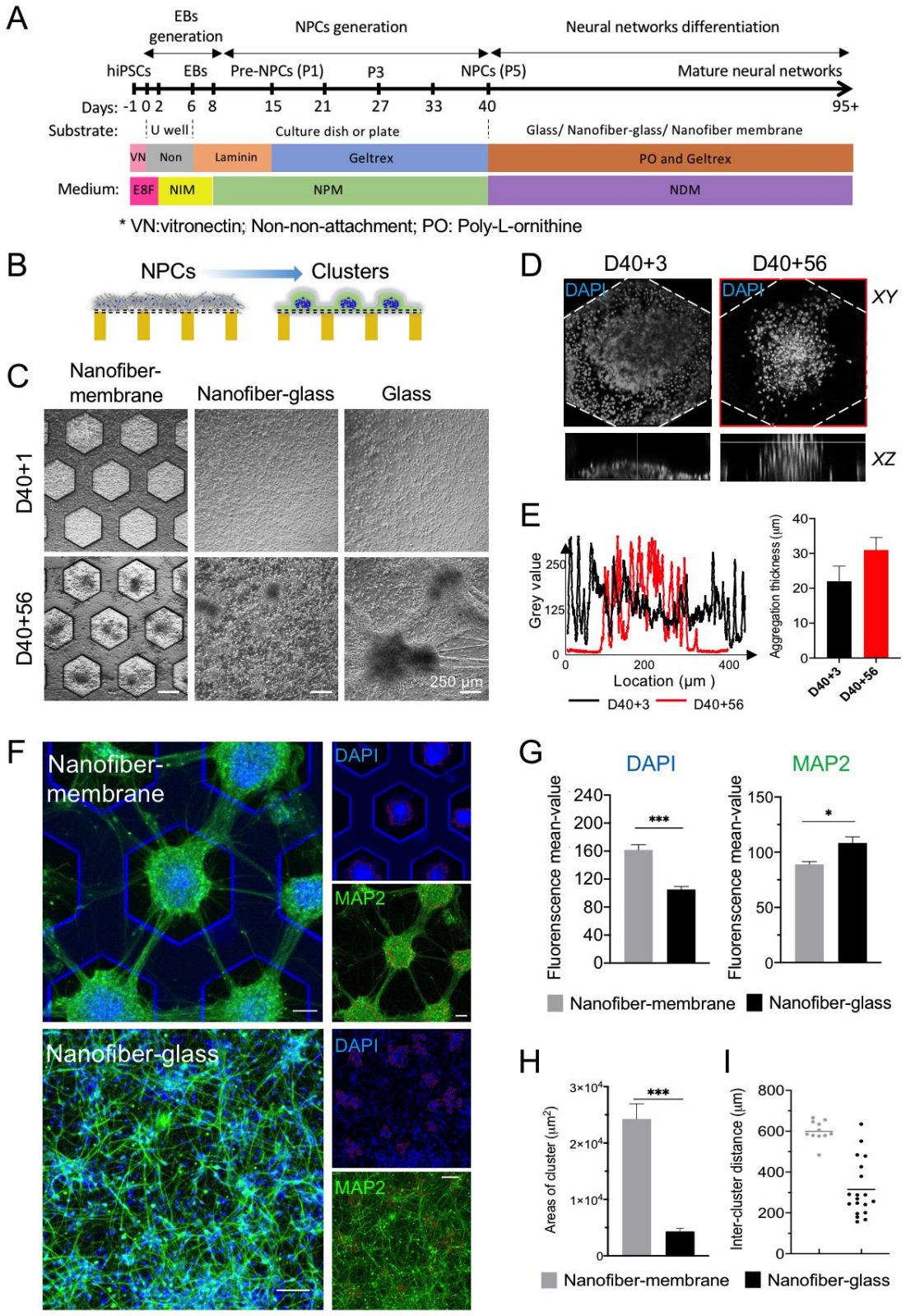
A
EBs generation
NPCs generation
Neural networks differentiation
hiPSCs
EBs
Pre-NPCs (P1)
P3
NPCs (P5)
Mature neural networks
Days: -1 0 2 6 8 15 21 27 33 40 95+
Substrate:
U well
Culture dish or plate
Glass/ Nanofiber-glass/ Nanofiber membrane
VN
Non
Laminin
Geltrex
PO and Geltrex
Medium:
E8F
NIM
NPM
NDM
* VN:vitronectin; Non-non-attachment; PO: Poly-L-ornithine
B
NPCs
Clusters
C
Nanofiber-membrane
Nanofiber-glass
Glass
D40+1
D40+56
250 μm
D
D40+3
D40+56
DAPI
XY
XZ
E
Grey value
Location (μm)
D40+3
D40+56
Aggregation thickness (μm)
F
Nanofiber-membrane
Nanofiber-glass
DAPI
MAP2
G
DAPI
MAP2
Fluorenscence mean-value
Nanofiber-membrane
Nanofiber-glass
H
Areas of cluster (μm²)
Nanofiber-membrane
Nanofiber-glass
I
Inter-cluster distance (μm)

Fig.3

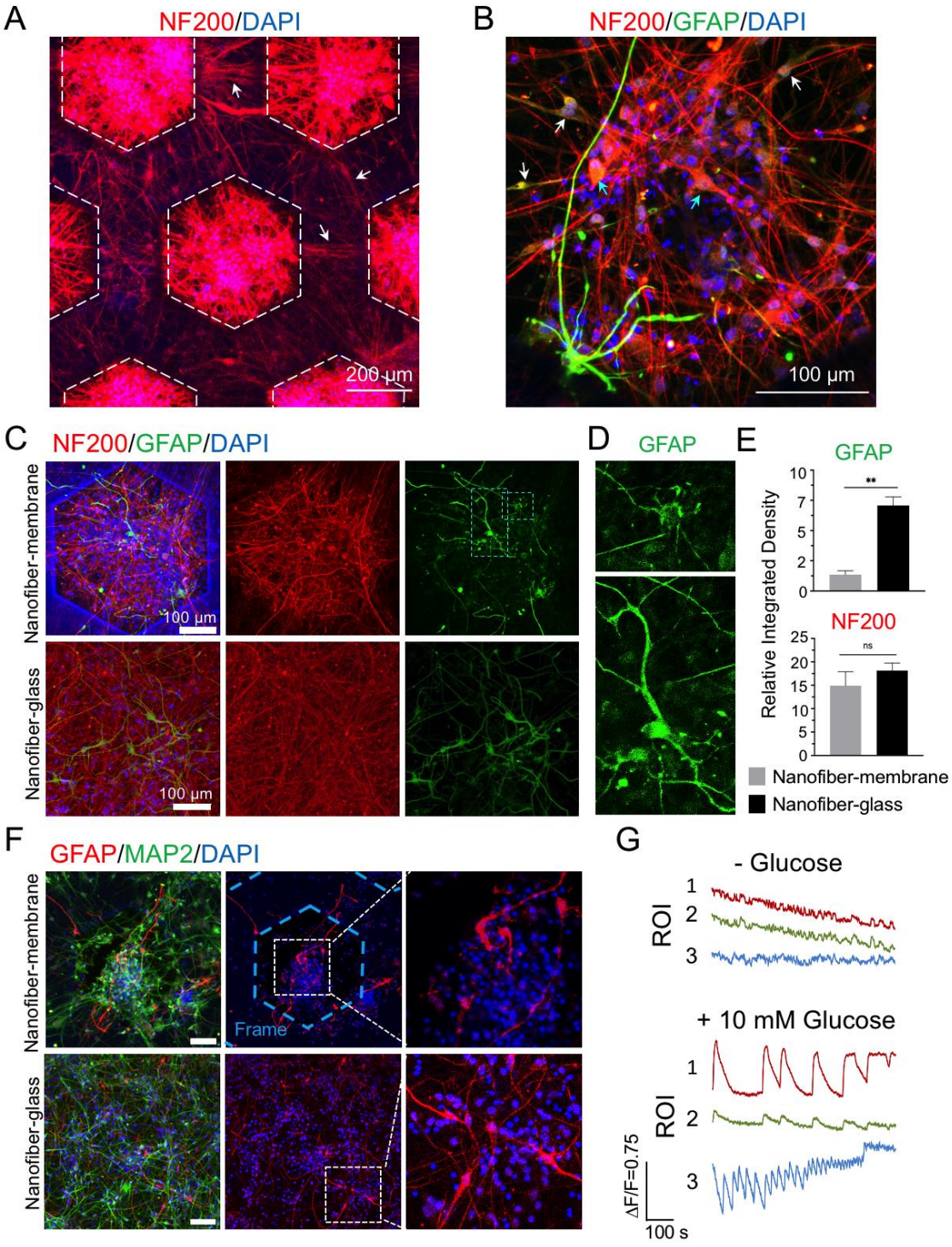
A
NF200/DAPI
200 μm
B
NF200/GFAP/DAPI
100 μm
C
NF200/GFAP/DAPI
Nanofiber-membrane
Nanofiber-glass
100 μm
100 μm
D
GFAP
E
GFAP
Relative Integrated Density
10
7
5
2
0
**
NF200
25
20
15
10
5
0
ns
Nanofiber-membrane
Nanofiber-glass
F
GFAP/MAP2/DAPI
Nanofiber-membrane
Nanofiber-glass
Frame
G
- Glucose
ROI
1
2
3
+ 10 mM Glucose
ROI
1
2
3
ΔF/F=0.75
100 s

Fig. 4

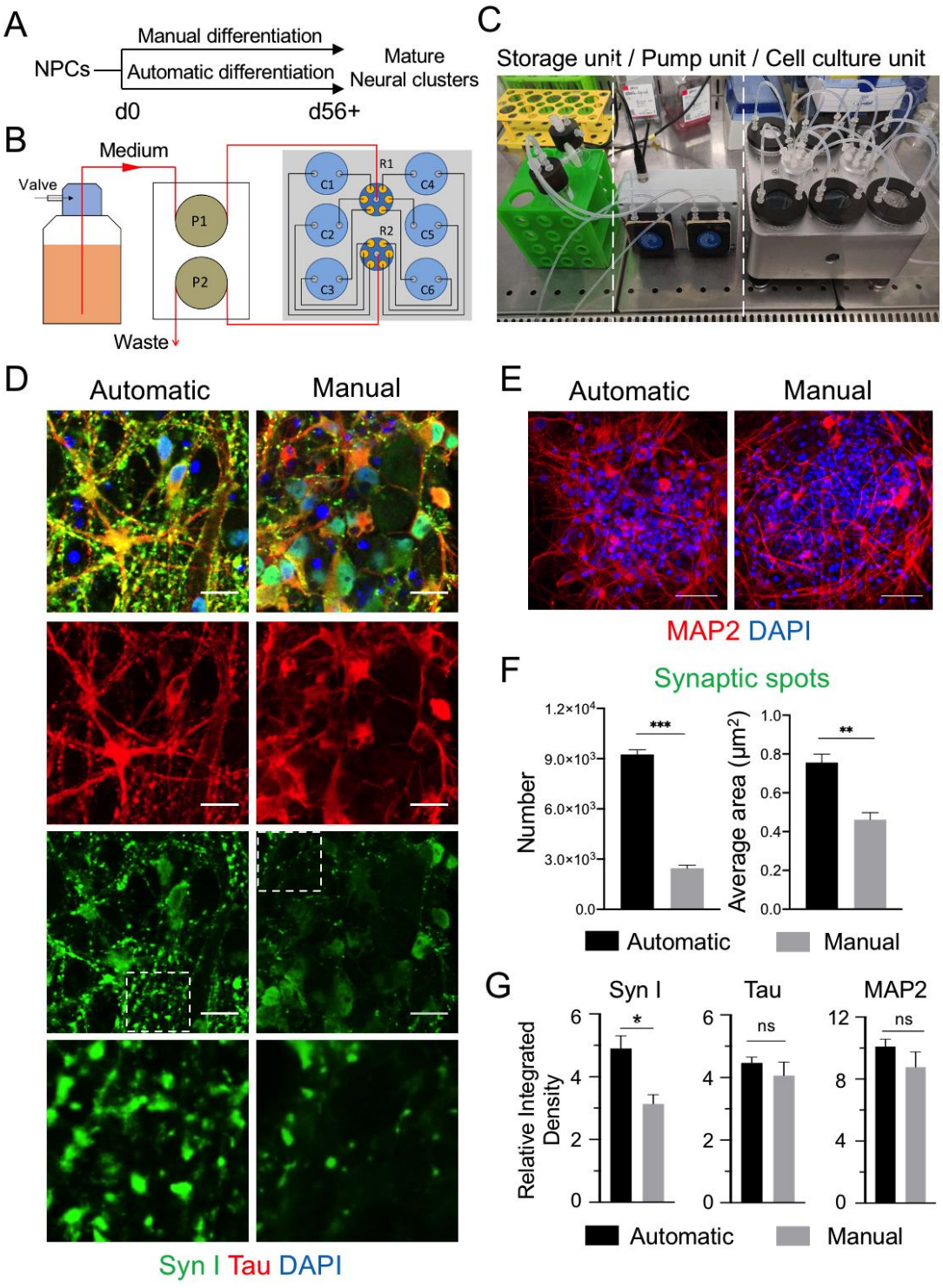
A
Manual differentiation
NPCs
Automatic differentiation
Mature
Neural clusters
d0
d56+
B
Medium
Valve
P1
P2
Waste
R1
R2
C1
C2
C3
C4
C5
C6
C
Storage unit / Pump unit / Cell culture unit
D
Automatic
Manual
Syn I Tau DAPI
E
Automatic
Manual
MAP2 DAPI
F
Synaptic spots
Number
Average area (μm²)
***
**
Automatic
Manual
G
Syn I
Tau
MAP2
Relative Integrated Density
*
ns
ns
Automatic
Manual

Fig. 5

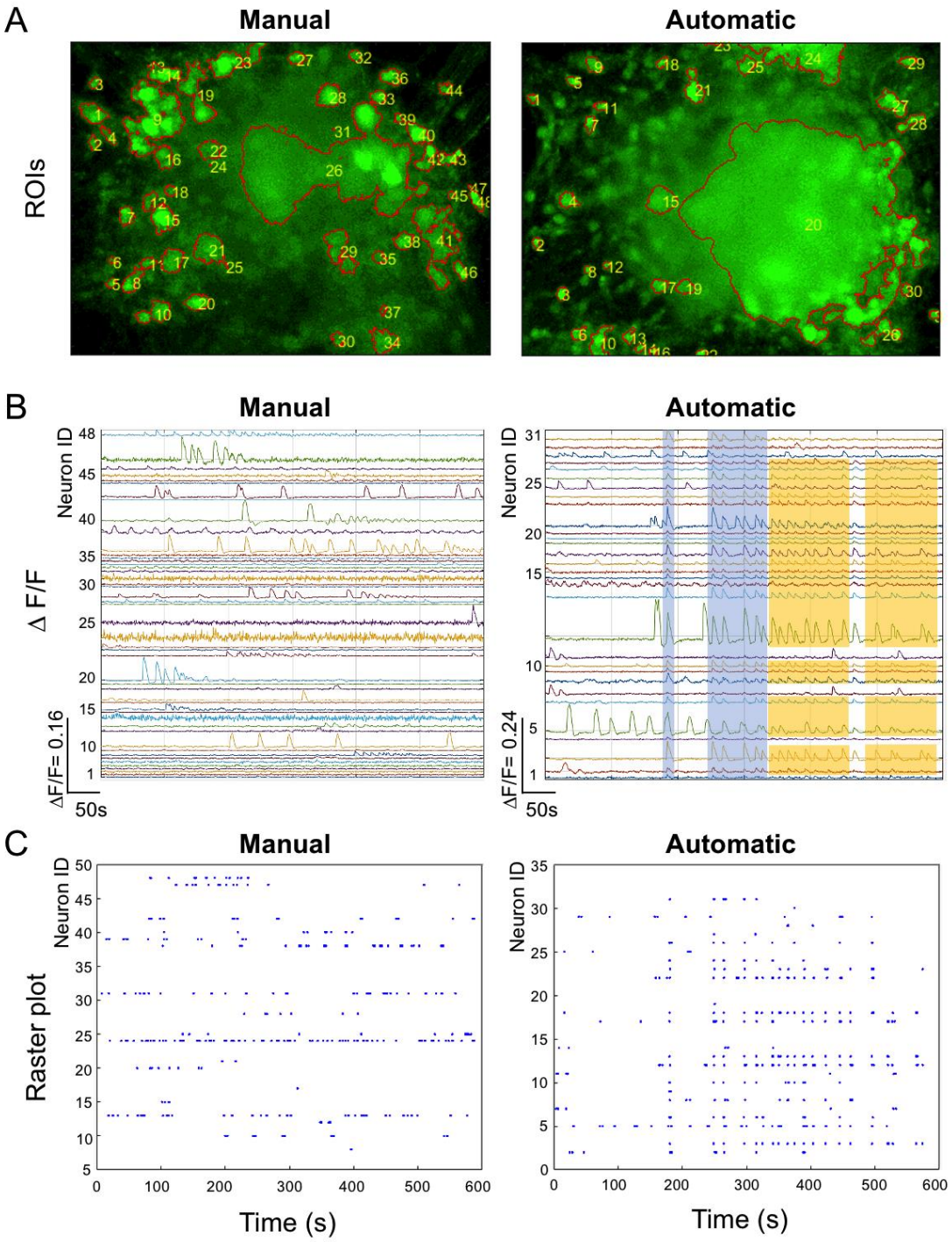
A
Manual
Automatic
ROIs
B
Manual
Automatic
Neuron ID
Δ F/F
ΔF/F= 0.16
ΔF/F= 0.24
50s
C
Manual
Automatic
Raster plot
Neuron ID
Time (s)